

ABSTRACT

Title of Dissertation: EFFECT OF LIPID-PROTEIN INTERACTIONS ON THE CONDUCTANCE OF THE TRANSMEMBRANE PROTEIN ALPHA HEMOLYSIN USING MOLECULAR DYNAMICS SIMULATIONS

Tejaswi Tammareddy, Master of Science, 2019

Dissertation directed by: Associate Professor, Dr. Jeffery Klauda,
Chemical and Biomolecular Engineering

Alpha-hemolysin (α HL) is a transmembrane ion-conducting channel which finds application in single molecule sensing using nanopore technology. Biomolecules are allowed to pass through the pore of the protein and, as a result, there is a change in the ion current, which is monitored to quantify single-molecule sensing. However, it has been established that the change in current is also affected by the lipid membrane in which the protein is present. It is also known that cholesterol has a concentration-dependent reduction in the current through the pore, experimentally. The understanding of current reduction at a single-molecule level and theoretical models replicating these conditions are lacking. In the current thesis, molecular dynamics simulations are performed on α HL inserted into a 1-palmitoyl-2-oleoyl-sn-glycero-3-phospho-choline (POPC) lipid bilayer with varying concentrations of cholesterol to investigate the effect on ionic current. Effect of lipid interactions, especially of cholesterol, on the protein structure and hence functioning of the ion channel is investigated.

EFFECT OF LIPID-PROTEIN INTERACTIONS ON THE CONDUCTANCE OF
THE TRANSMEMBRANE PROTEIN ALPHA HEMOLYSIN USING
MOLECULAR DYNAMICS SIMULATIONS

by

Tejaswi Tammareddy

Dissertation submitted to the Faculty of the Graduate School of the
University of Maryland, College Park, in partial fulfillment
of the requirements for the degree of
Master of Science
2019

Advisory Committee:

Dr. Jeffery Klauda, Chair

Dr. Amy Karlsson, Assistant Professor

Dr. Ganesh Sriram, Associate Professor

© Copyright by
Tejaswi Tammareddy
2019

Dedication

I would like to dedicate this thesis to my family, especially my sister, without whose love, encouragement and support, none of this would have been possible.

Acknowledgments

I would like to use this opportunity to express my utmost gratitude to my advisor, Dr. Jeffery Klauda, for providing me with this valuable chance to take up this project. I would like to thank him for being extremely patient and supportive throughout the project and teaching me the minute details required to be a researcher that is often overlooked and for pointing me in the right direction whenever faced with a problem.

I would also like to show my gratitude and appreciation to Nick Guros for his advice and guidance whenever required. I would like to appreciate him for patiently clarifying and bearing up with the many questions I had, time and again.

Lastly, I would like to appreciate the faculty of Chemical and Biomolecular Engineering, from whom I have learned a great deal of stuff through the course work and in person while pursuing the research interests I have.

Table of Contents

Dedication.....	ii
Acknowledgements.....	iii
Table of Contents.....	iv
List of Tables	v
List of Figures	vi
List of Abbreviations	viii
Chapter 1: Introduction.....	1
Chapter 2: Methods.....	8
Chapter 3: Results.....	16
Chapter 4: Discussion.....	36
Chapter 5: Conclusion and Future Work.....	39
References.....	40

List of Tables

Table 2.1 Initial parameters of the systems simulated

Table 3.1 Current through the pore of various systems in pA.

List of Figures

Figure 1.1 showing the structure of the protein α -hemolysin

Figure 1.2 depicting the chemical structure of the lipids POPC and Cholesterol

Figure 2.1 showing the steps involved in building bilayer systems using CHARMM-GUI

Figure 3.1. A, B, and C depicting the images of the 10%, 30%, and 50% systems respectively, before performing equilibration

Figure 3.2. A, B and C showing the surface area/lipid values plotted as a function of time for the three replicas of 10%, 30%, and 50% cholesterol systems, in POPC bilayer system

Figure 3.3. A, B and C showing the RMSD Vs time for various replicates of the 10%, 30%, and 50% Cholesterol systems, in the NPT process

Figure 3.4 showing the structure of pore and constriction points 1 & 2 for the ion flow

Figure 3.5 showing the *trans*-entrance of the first replica of 50% cholesterol system **A)** before the simulation **B)** and channel occlusion after the electric field is applied.

Figure 3.6. A, B and C showing the pore radius profiles for the three replicates of the 10% Cholesterol system in the NPT process during the 200ns equilibration

Figure 3.7. A, B and C showing the pore radius profiles for the three replicates of the 30% Cholesterol system in the NPT process during the 200ns equilibration

Figure 3.8. A, B and C showing the pore radius profiles for the three replicates of the 50% Cholesterol system in the NPT process during the 200ns equilibration

Figure 3.9 showing the pore occlusion in replicate-1 of 50% cholesterol system with charged residues at the *trans*-entrance of the pore (constriction point 2) bending inwards, thereby obstructing the ion flow

Figure 3.10 showing the pore radius profiles for the three replicates of the 10% Cholesterol system in the NVT process with the electric field on

Figure 3.11 showing the pore radius profiles for the three replicates of the 30% Cholesterol system in the NVT process with the electric field on

Figure 3.12 showing the pore radius profiles for the three replicates of the 50% Cholesterol system in the NVT process with the electric field on

Figure 3.13 showing the net current accumulation for the three replicates of the systems simulated in the NVT process

List of Abbreviations

POPC- 1-palmitoyl-2-oleoyl-sn-glycero-3-phospho-choline

DPhPC- 1,2-diphytanoyl-sn-glycero-3-phospho-choline

MD simulations- Molecular dynamics simulations

PC- phosphatidylcholine

PS- phosphatidylserine

PE- phosphatidylethanolamine

SM- sphingomyelin

NMR- Nuclear magnetic resonance

DNA- Deoxyribonucleic acid

RNA- Ribonucleic acid

α HL-Alpha Hemolysin

pA- Pico amperes

CHARMM-GUI- Chemistry at Harvard Macromolecular Mechanics-Graphic User
Interface

NAMD- Nanoscale Molecular Dynamics

VMD- Visual Molecular Dynamics

RMSD- Root mean square deviation

PME-Particle mesh Ewald

Chapter 1: Introduction

1.0 Cell membrane

The cell membrane separates the components of the cell from that of the environment. It is essentially composed of lipids arranged in the form of a bilayer with proteins embedded in it. There are various types of lipids which perform different functions such as lipids that store energy in the form of lipid droplets, polar lipids involved in the spontaneous formation of membranes and lipids involved in signaling and molecular recognition of cells. Polar lipids forming the membrane (phospholipids) are *amphipathic* with a hydrophilic head part and hydrophobic tails. Due to the interactions with a surrounding aqueous environment, hydrophobic tails spontaneously assemble into a bilayer exposing the hydrophilic head part to the water content in and outside of the cells thereby forming a membrane.^{1,2} There can exist thousands of lipid molecular types spanning the different cell membranes of various cells. More than half of the membrane lipids are made of four phospholipids namely phosphatidylcholine (PC), phosphatidylserine (PS), phosphatidylethanolamine (PE), and sphingomyelin (SM). Apart from the phospholipids, there are glycolipids and cholesterol for the rest of the membrane lipids in varying concentrations.³ All the lipids are arranged as a bilayer in the membrane and the lipids, as well as proteins, diffuse laterally within the membrane.⁴ Due to the presence of a hydrocarbon ring in the structure of cholesterol, it interacts with the tails of the neighboring lipids in the membrane. These interactions are interesting to study because cholesterol exhibits an increase or decrease in the

overall fluidity of the membrane, depending on the temperature and lipid type in the membrane.¹

Although lipids form the basic structural components in the cell membrane, membrane proteins play an important role in performing various functions of the cell. Depending on the structural organization, there are two types of proteins associated with the lipid bilayer namely transmembrane proteins and peripheral proteins. Peripheral proteins interact with the surface of one side of a lipid membrane while trans membrane proteins are either partially or completely buried in the bilayer. Like the phospholipids, transmembrane proteins also exhibit amphiphilic nature with some portion of the protein being hydrophobic while the remaining is hydrophilic.⁵ Proteins in the membrane either act as receptors or transporters. Transporters are further classified as a channel forming proteins or active transporters. Active transporters can carry molecules against an electrochemical gradient while channel/pore-forming proteins detect and allow only specific molecules or ions to pass through.⁶ Channel/pore-forming proteins enable transport by selectively identifying and transporting the molecules down a chemical or concentration gradient.⁷ These pore-forming proteins have pore sizes in the range of a few nanometers and find applications in biosensors. For instance, the structure of a protein can be characterized by using X-ray crystallography, nuclear magnetic resonance (NMR) spectroscopy, infrared spectroscopy, circular dichroism, etc.

1.1 Analyte detection and pertinence of alpha-hemolysin

Similar to the proteins present in a cell there is a wide range of biomolecules that participate in many biological processes. Understanding and characterizing the structure, as well as dynamics of these process, would be of great use in many biomedical or biotechnological applications. Similar to the protein structure determination techniques, there are experimental methods available for DNA or RNA sequencing such as Sanger's method (first generation sequencing) and next-generation sequencing techniques such as Illumina, Roche, etc. But these techniques use bulk sampling and obtaining the process dynamics at a single molecule level, is lacking. To address this shortcoming, single-molecule-sensing techniques have been developed as a third generation sequencing methods.⁸

These single-molecule-sensing techniques require nanopores for high-sensitivity, single-molecule detection of the macro-sized biomolecules. Transmembrane proteins offer a great advantage over synthetic pores for sequencing, due to their availability of pores in the size of a few nanometers. These nanopores have an additional advantage in detecting the biomolecules, which are at low concentrations where bulk characterization is not possible.

The underlying principle of nanopores is that of a Coulter counter, which was initially used to count the number of blood cells in a fluid. This is achieved by characterizing the size of a micron-sized particles by allowing them to pass through a micro-sized aperture.^{9 10} When an electric field is applied across the pore of the molecule, it generates an electric potential across the pore and drives any charged molecules to pass through the pore, individually, obstructing the ionic current across

the channel.^{11, 12} This change in the current across a constriction point (in the range of pico-amperes) in the nanopore, could be used to characterize the biomolecule.

There are three types of nanopores available, namely, biological nanopore, synthetic or material-based nanopores and hybrids of biological and synthetic nanopores. Biological nanopores are usually the proteins (such as a transmembrane protein α -hemolysin (α HL))¹³ with pore sizes in the nanoscale and useful in characterization of biomolecules. Synthetic nanopores are a good alternative to biological nanopores, such as, silicon-based substrates, graphene-based nanopores, aluminum oxide based nanopores, etc.¹⁴ Material-based nanopores possess the advantage of having known geometries and ease of controllability of structural properties.¹⁵ Hybrid nanopores are built from incorporating α HL into synthetic substrates.¹⁶ Synthetic and hybrid nanopores have limitations in terms of stability which depends on the conditions used to form the nanopores.⁸

Although material-based nanopores have advantages, biology has many examples of nanopores. The first transmembrane protein to be used as a nanopore is α -hemolysin, which is generated by a bacterium *Staphylococcus aureus*. This protein has been demonstrated to the sequence of single-stranded DNA when it was passed through its pore. Another commonly used nanopore is a protein aerolysin produced by *Aeromonas hydrophila* which also has a similar structure to that of α HL.¹⁷

α HL is a heptameric protein which assembles spontaneously on cell membranes. It has a mushroom-shaped structure with a head part in the diameter range of 100 Å and a total height of 100 Å. Pore region of the protein has a pore diameter of 1.9 Å, which is composed of 14 (2 contributed by each monomeric unit) antiparallel β -

strands. Interior of this β -barrel structure is hydrophilic while the exterior is a hydrophobic surface because of which it inserts into the lipid membranes and forms pores. It is also called α toxin, due to its nature of spontaneously inserting into the membranes thereby forming pores and causes osmotic swelling of the cells followed by cell death. Figure 1.1 indicates the structure of α HL.^{18,19}

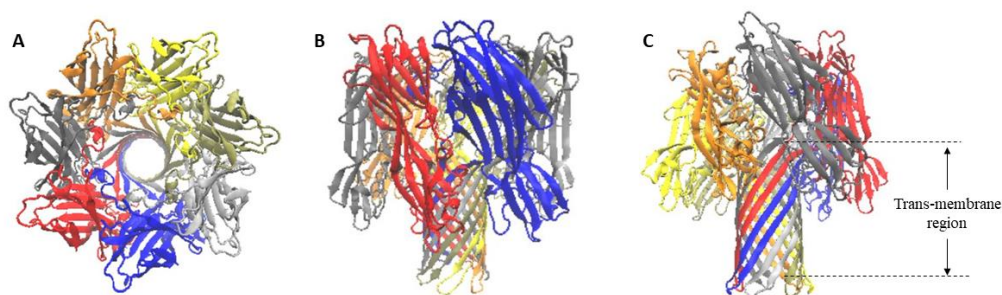


Figure 1.1 The structure of the protein α - hemolysin²⁰. **A)** Top view of the protein showing the pore and heptameric assembly structure with each monomeric unit represented by a different color. **B)** Front view of the protein showing the mushroom-like structure with a head part and a stem part that inserts into the membrane **C)** protein oriented to show the structure of the transmembrane region, composed of two β -sheets contributed by each monomeric unit and connected by a hairpin loop at the trans-entrance of the protein. Protein figures captured using VMD.²¹

1.2 Importance of lipid interactions

Since α HL has the potential to be used in nanopore technologies, measuring the changes in current should be accurate for the sensitivity of analyte detection through the pore. It has been established by Guros et al.²² that lipid type, in which α HL is inserted into, has an effect on the ionic current through the pore. They performed MD simulations on α HL inserted into 1,2-diphytanoyl-sn-glycero-3-phospho-choline (DPhPC) and 1-palmitoyl-2-oleoyl-sn-glycero-3-phospho-choline (POPC) and compared the effect of lipid type on the ionic conductance. Although DPhPC and POPC are similar in structure, DPhPC has a better match of the hydrophobic thickness of the

protein. This hydrophobic match was essential in maintaining the proper alignment of β -sheet loops, at the end of the pore in α HL, and enabled a stable channel formation. They also found out that the ion current through the pore in DPhPC is almost 1.5 times greater than that in POPC, while also showing a good agreement of the simulations to that of experimental data. This highlights the importance of lipid type and protein-lipid interactions in the functioning of α HL.

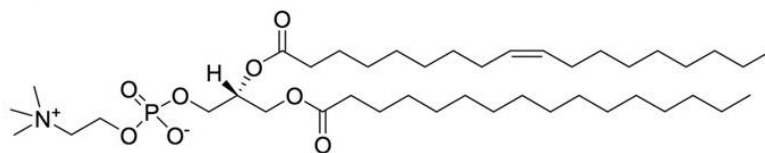
It has been established previously¹³ that there is a difference in the conductance of the current through the pore between PC and a combination of PC and PS lipids. Also, Valenzuela et al.²³ studied the effect of different cholesterol concentrations on the conductance of α HL as well as a chloride ion-conducting channel CLIC1. They found out that the conductance of α HL varied in a concentration-dependent manner experimentally. Hence it would be interesting to understand the molecular-level lipid-protein interactions that are responsible for the change in conductance.

1.2 Role of cholesterol and the overall idea of the project

Due to the presence of a hydrocarbon ring in the structure of cholesterol as shown in Figure 1.2, interactions with the neighboring lipids or the protein will be different from that of POPC and is a topic of interest for many researchers. Since the protein α HL inserts into the membrane spontaneously, the change in fluidity in the membrane might affect the formation and sustainability of pore in the membrane. It has been established by Valenzuela et al.²³ that cholesterol has a regulatory effect on another bacterial pore-forming protein, i.e. CLIC1. They not only found out that the conductance through the pore of α HL is reduced due to the presence of cholesterol in

the membrane but also observed the change to be concentration dependent. Although they were able to establish the reduction in current, it is not clear whether it is because of a reduced protein insertion and assembling or change in conducting state. To fill the gaps in understanding at a molecular level, which in turn enables in improving the sensitivity of nanopore technologies, molecular dynamics simulations could be used. To understand the effect of cholesterol on the structure and hence functioning of α HL, molecular dynamics simulations are performed, and the results are tabulated in the following sections.

A) POPC



B) Cholesterol

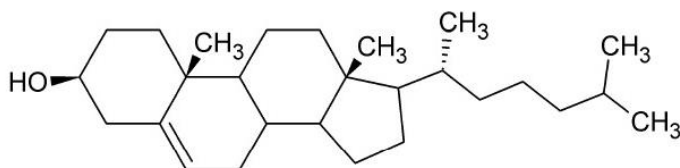


Figure 1.2 depicting the chemical structure of the lipids A) POPC with unsaturated lipid tails and B) Cholesterol with its hydrocarbon ring structure

Chapter 2: Methods

2.1 Molecular dynamics simulations

Molecular dynamics (MD) simulation is a powerful tool in predicting the interactions of all atoms in a system as a function of time. This technique finds application in studying the structure, function, and processes of biomolecules such as protein folding/unfolding, conformational changes of a molecule, and protein insertion into a membrane.²⁴ Biological processes such as these occur at a nanosecond, microsecond or even higher timescale whereas MD simulations for all-atom simulations requires integration timesteps of a femtosecond, which requires millions of steps to simulate a process on the nanosecond timescale. It works by generating the coordinates, velocities and thereby generating the trajectories of all the atoms in the system.²⁵

The underlying principle in MD simulations is that the force experienced by each atom due to every other atom in the system can be calculated by solving Newton's Laws of motion, numerically, as in equation $F_i = m_i a_i$ where i represent the i^{th} particle in the system²⁶. MD simulations take into account the initial positions of the atoms in the system and initial velocities. It then computes all the forces experienced and updates for each timestep the velocities and coordinates. The forces generated by atom-atom interactions are usually represented in terms of position-based potential functions as shown in equation 2.1.²⁷

$$\begin{aligned}
E = & \sum_{bonds} \frac{a_i}{2} (l_i - l_{i0})^2 + \sum_{angles} \frac{b_i}{2} (\theta_i - \theta_{i0})^2 + \sum_{torsions} \frac{V_n}{2} (1 + \cos(\eta\omega - \gamma)) \\
& + \frac{1}{2} \sum_{i=1}^N \sum_{j \neq i}^N 4\varepsilon_{ij} \left[\left(\frac{\sigma_{ij}}{r_{ij}} \right)^{12} - \left(\frac{\sigma_{ij}}{r_{ij}} \right)^6 \right] + \frac{1}{2} \sum_{i=1}^N \sum_{j \neq i}^N \frac{q_i q_j}{r_{ij}}
\end{aligned}
\tag{0.1}$$

In the equation, l_i denotes bond length, l_{i0} denotes equilibrium bond length; θ_i represents bond angle and θ_{i0} denotes the equilibrium bond angle; ω represents the dihedral angle; V_n represents the barrier height; γ represents phase shift in n-fold term; ε represents the strength of attraction between two particles (well depth); σ_{ij} is the distance between particle i and particle j where the interatomic potential is zero; r_{ij} is distance between the n particles i and j; q_i and q_j are charges for particles at i and j respectively.

The two types of interactions computed in a typical MD simulation are bonded interactions and non-bonded interactions and are together known as the molecular mechanics force field. Bonded interactions include bond length, dihedrals, and torsional angles while non-bonded interactions include van der Waals and Coulomb's electrostatic interactions. In equation 2.1, the first three terms represent bonded interactions and deal with internal degrees of freedom within the molecules. The first term in the equation calculates the energy change associated with the bond length changing to l_i from the equilibrium value l_{i0} . The second term calculates the energy change caused by a change in the bond angles. Similarly, the third term evaluates torsional potential caused by bond rotations. The fourth term represents the van der

Waals force estimated by the Lennard-Jones potential. The fifth term represents the electrostatic potential caused by Coulombic interactions. In the expression 2.1, the first four terms represent short-ranged interactions while the fifth term is a long-ranged potential. The MD method essentially generates three-dimensional trajectories of the atoms in the system with respect to each other. MD simulations provide a major advantage of understanding and controlling the conditions of the simulation accurately such as conformational states, surrounding environment, perturbations like experimental conditions, in a system.²⁵

There are various steps involved in performing an MD simulation. In most cases involving proteins with membranes, these steps include having the known structure of the protein, building the protein-membrane systems, allowing the system to equilibrate, performing production runs followed by the analysis of results. In the current thesis, structural data of the transmembrane protein α HL²⁰ is downloaded from the protein data bank (RCSB ID-7AHL). Since the protein is a transmembrane protein, to avoid artifacts introduced through X-ray crystallography (low temperature and non-native environments), simulations are performed in a well-hydrated lipid environment and allowed to relax and equilibrate.²⁶ After initial equilibration, production runs are performed in constant pressure and temperature process (NPT) to stabilize lipid packing and the ion conductance values through the pore of α HL are carried out in constant volume and temperature process (NVT). A more detailed explanation of the methods used in the current thesis is in the following subsections.

2.2 Building the membrane-protein system

All-atom molecular dynamics simulations are performed on α HL protein inserted into POPC and cholesterol membranes with varying lipid concentrations. In this project, three different protein-membrane systems of α HL are built into POPC lipid membrane with 10%, 30% and 50% of cholesterol concentrations and their results are reported. The experimental data on ion conductance pertaining to these cholesterol concentrations are available in Valenzeula et al.²³ to compare and analyze. Each system has three replicas built and simulated for the consistency of results.

The CHARMM-GUI *Membrane Builder*²⁸⁻³⁰ (Graphic user interface of the software CHARMM) was used to build the membrane-protein systems.³¹ There are five steps involved in building the membrane system using CHARMM. In the first step, the protein structure is read and necessary modifications to the protein such as removing residues could be performed. In the current case, no such modifications were required. In the second step, the protein is oriented along the z-direction to align properly with respect to the lipid bilayer. In this step, the cross-section of the protein along the z-direction is calculated and could be used to align the planes between which lipid bilayer would be inserted. In the third step, lipid composition options are available in which the ratio of lipids (POPC and cholesterol) is used to measure the size of the system from an initial guess is calculated along X and Y direction. Water thickness determines the size along Z-direction. In the fourth step, components of the system (lipids forming a bilayer around the protein, water molecules, and ions) are generated. Many KCl ions, contributing to a 4M concentration, were generated in all the systems to simulate the conditions similar to those in experiments. In the fifth step, the generated components

are assembled. The system thus generated is energy minimized for bad contacts and equilibrated using software NAMD, in section 2.3.

In the current thesis, PDB ID for the protein of choice is 7AHL which is read from RCSB³² database and used for building the system. A total of 9 systems were built with varying concentrations of cholesterol and POPC lipids. Systems were built in a tetragonal box with sufficient water thickness to keep the membranes well hydrated. TIP3P water model^{33 34} was used with the C36 force fields for the protein and lipids.^{35 36} Insertion method was used for placing the components.³¹

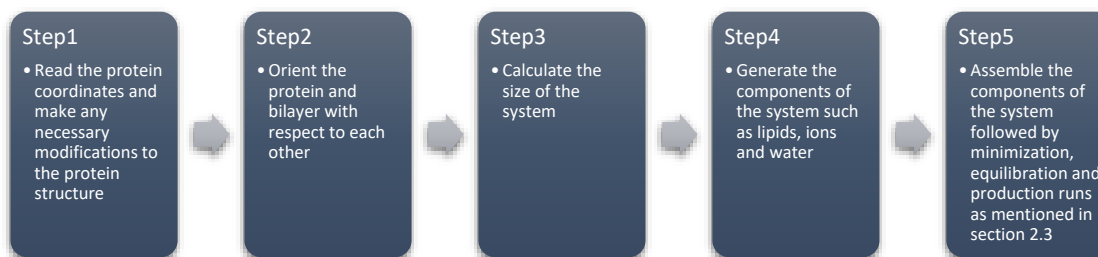


Figure 2.1 showing the steps involved in building bilayer systems using CHARMM-GUI

2.3 Equilibration and production runs

Components of the system assembled in the previous steps are required to be verified for bad contacts. For example, there may be lipid molecules penetrating the other lipids or into the protein. Hence, it is required to perform energy minimizations to resolve bad contacts. Distance between two atoms serves as a good criterion to detect bad contacts and a distance $<1.2\text{\AA}$ is considered to be a bad contact. Lipid-lipid bad contacts can be easily resolved in this minimization step, but the bad contacts involving lipid tails entering the ring in the cholesterol cause unusual bond lengths and bond energies. CHARMM-GUI resolves these bad contacts by translating the cholesterol

molecule and performing minimizations to the surrounding lipids (keeping everything else fixed) and translating back the cholesterol molecule to its position. If this minimization does not resolve the bad contacts, bilayer needs to be built again.²⁹

For the assembled components to relax and stabilize to carry out the production runs, equilibration steps need to be performed. CHARMM-GUI generates the input files required for the various steps of equilibration after the components are assembled in step5. There are six equilibration steps and each step have different restraints added to lipids, protein, water, and ions. First two steps are NVT (constant volume, temperature) and rest of the four steps are performed in NPAT (constant pressure, area, temperature) process. Three different types of restraints are applied to various components of the system in each step. Positional harmonic restraints are added to the protein backbone, sidechains, and ions in the system. Repulsive planar restraints are added to prevent water from entering the membrane hydrophobic region. Planar restraints are used to hold the lipid head groups in position along the Z axis and lipid tails to remain buried inside. The intensity of these restraint forces reduces gradually through the steps. Force constants applied in each step for the lipids are described in further detail in Jo et al.³¹

The standard CHARMM-GUI 6-step equilibration and minimization is followed by production runs, both simulated in this work, with the NAMD program³⁷. In the current thesis, an additional 200ns equilibration step is performed under semi-isotropic conditions (NPT) before applying the electric field to the systems. The Nosé-Hoover Langevin-piston algorithm^{38 39} was used to perform NPT simulations. Surface area/lipid values were monitored to ensure that the membrane equilibrated and then the

simulations were run under constant volume conditions (NVT), for 200ns with an additional 50ns in systems that have shown fluctuations in the properties, for accuracy. A uniform electric field of -40mV is applied along the Z axis. The van der Waals interactions were smoothly switched off between 10 Å and 12 Å by a force-based switching function⁴⁰. All the bond lengths involving hydrogen atoms were constrained using SHAKE algorithm⁴¹. Particle mesh Ewald (PME) method⁴² was used for electrostatic interactions in the interpolation order of 6 and a direct space tolerance of 10^{-6} . Table 2.1 provides the details on the various systems built and used for analysis.

Table 2.1 Initial parameters of the systems simulated.

System	# of lipids	# of water molecules	Initial cell dimensions [Å]	Simulation time [ns] with NPT	Simulation time [ns] with NVT
10% Chol system	467	59888	A = 134.818 B = 134.818 C = 162.704	200	Run1-200 Run2-200 Run3-200
30% Chol system	324	38220	A = 111.723 B = 111.723 C = 62.704	200	Run1-250 Run2-200 Run3-200
50% Chol system	360	38945	A = 112.401 B = 112.401 C = 162.704	200	Run1-200 Run2-200 Run3-250

2.4 Analysis of results and visualization

While running the simulations in the NPT process, the surface area was calculated and plotted with respect to the time of simulation to make sure that it reaches a stable value. Area per lipid calculations was carried out by taking the area in XY plane, where the lipids were assembled to form a bilayer and the approximate cross-sectional area of the protein pore is subtracted (1018 \AA^2) followed by dividing it by the number of lipids. A running average of the surface area is also calculated to better

understand the trend in the progress of the simulation and when the value did not change by 0.5 \AA^2 , the membranes were considered equilibrated.

Concurrently, to monitor the protein structural changes, root mean square deviation (RMSD) and pore radius profiles were also evaluated. RMSD was determined in CHARMM³⁰ using CORREL command with the initial structure of the protein as the reference. Hole program⁴³ was used to determine the radius of the pore along the Z axis.

Ion conductance through the pore of the protein was performed on the reentered trajectories to take into account the diffusion of the protein itself, within the membrane. CHARMM was used to evaluate the accumulation of the ions (K^+ and Cl^-) across the center of the membrane. Current through the channel is calculated (in picoamperes) as per the equation 2.2 and plotted with respect to time of the simulation.

$$i = \frac{(N_{\text{K}^+} - N_{\text{Cl}^-})q}{\Delta t} \quad (0.2)$$

Visual Molecular Dynamics (VMD) software²¹ was used to view the trajectories generated as well as to capture the relevant snapshots in the simulation.

Chapter 3: Results

3.0 Building the membrane protein systems

Protein-membrane systems were built using CHARMM-GUI³⁰ as described in the previous chapter. Figure 3.1 contains snapshots of the systems built and the images after the standard 6-step equilibration process. In Figure 3.1, protein α HL, which has a mushroom-like shape, is aligned along Z-axis and the lipid bilayer is placed in the XY plane. The transmembrane region of the protein is inserted into the membrane while the head part of the protein remains outside. Although water molecules are not shown, the entire system is well solvated and is built in a tetragonal box. As shown in figure 3.1, protein is placed at the center of the lipid bilayer composed of POPC lipids (represented in cyan) with cholesterol molecules embedded in it. From the figure, all the hydrophobic lipid tails from the upper leaflet are facing those from the lower leaflet, thereby avoiding contact of water molecules and forming a bilayer. Lipid heads towards the head of the protein fall in the extracellular aqueous environment while the lipid heads at the bottom of the protein pore region fall in the intracellular aqueous environment. Cholesterol molecules are scattered throughout the POPC bilayer to make up to the required concentrations in each system. Increase in the cholesterol concentration in the systems is evident from the increase in the number of cholesterol molecules (represented in red). While assembling the components of the system (protein, lipids, ions and water molecules), lipids interact with neighboring lipids as well as with protein, and this can cause a tilt in the angle at which the protein is inserted (evident from Figure 3.1 (B and C) as compared to 3.1 A).

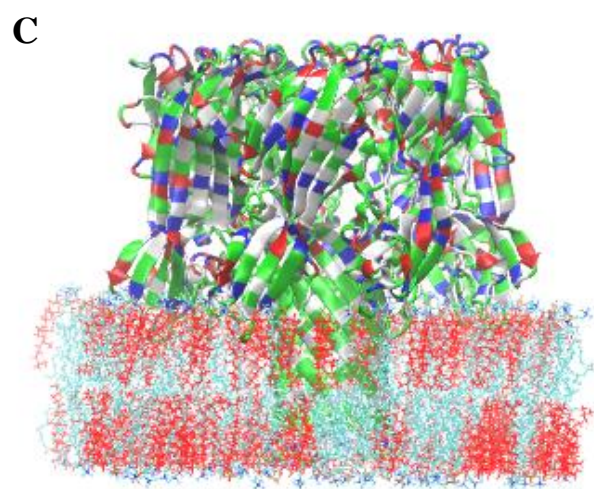
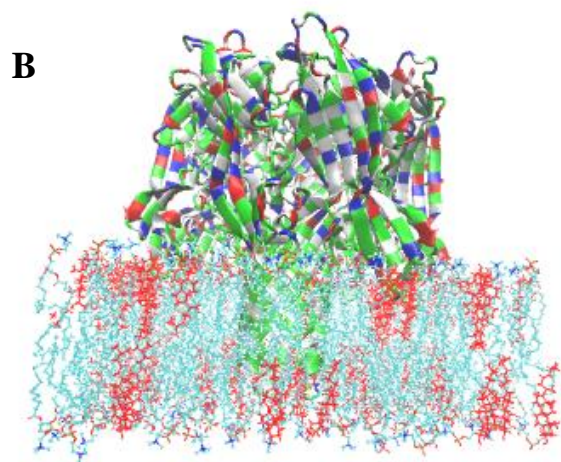
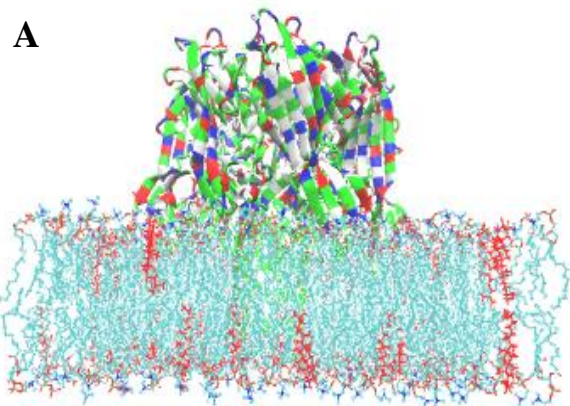


Figure 3.1. A, B, and C depicting the images of the 10%, 30% and 50% systems respectively, before performing equilibration. Protein represented as cartoon colored based on type of residue. Lipid bilayer composed of POPC-represented in cyan and Cholesterol-represented in red. Water molecules are not shown in the representation.

3.1 Testing equilibration of the bilayer-protein systems

To test the equilibration of the systems under consideration, a 200ns equilibration was performed under the NPT process. It was found by Guros et al.²² that the equilibration time of 200ns was required for the system to stabilize and that this additional equilibration before applying electric field has contributed to the results close to experiments. Also, the surface area per lipid is proven to be a better measure for equilibration than the energy criteria in systems involving an ion channel. Surface area per lipid (subtracting out the protein) is calculated at regular intervals and plotted against time in Figure 3.2. Three replicates at each concentration of cholesterol (10%, 30%, and 50%) were performed and the results were plotted.

There is good consistency observed in the three replicas of each system and converged to a near-constant value, but the area to which 10%, 30%, and 50% cholesterol system converged are different. From Figure 3.2, it is evident that the surface area at which the systems equilibrated reduced with the increase in the cholesterol concentration of the membrane. The surface area at which the membranes equilibrated reduced from $68.8 \pm 0.5 \text{ \AA}^2$ in 10% system to $57.8 \pm 0.6 \text{ \AA}^2$ in 50% cholesterol system. This reduction in the area might be because of the lipid rearrangement (packing) with respect to the other lipids as well with the protein.

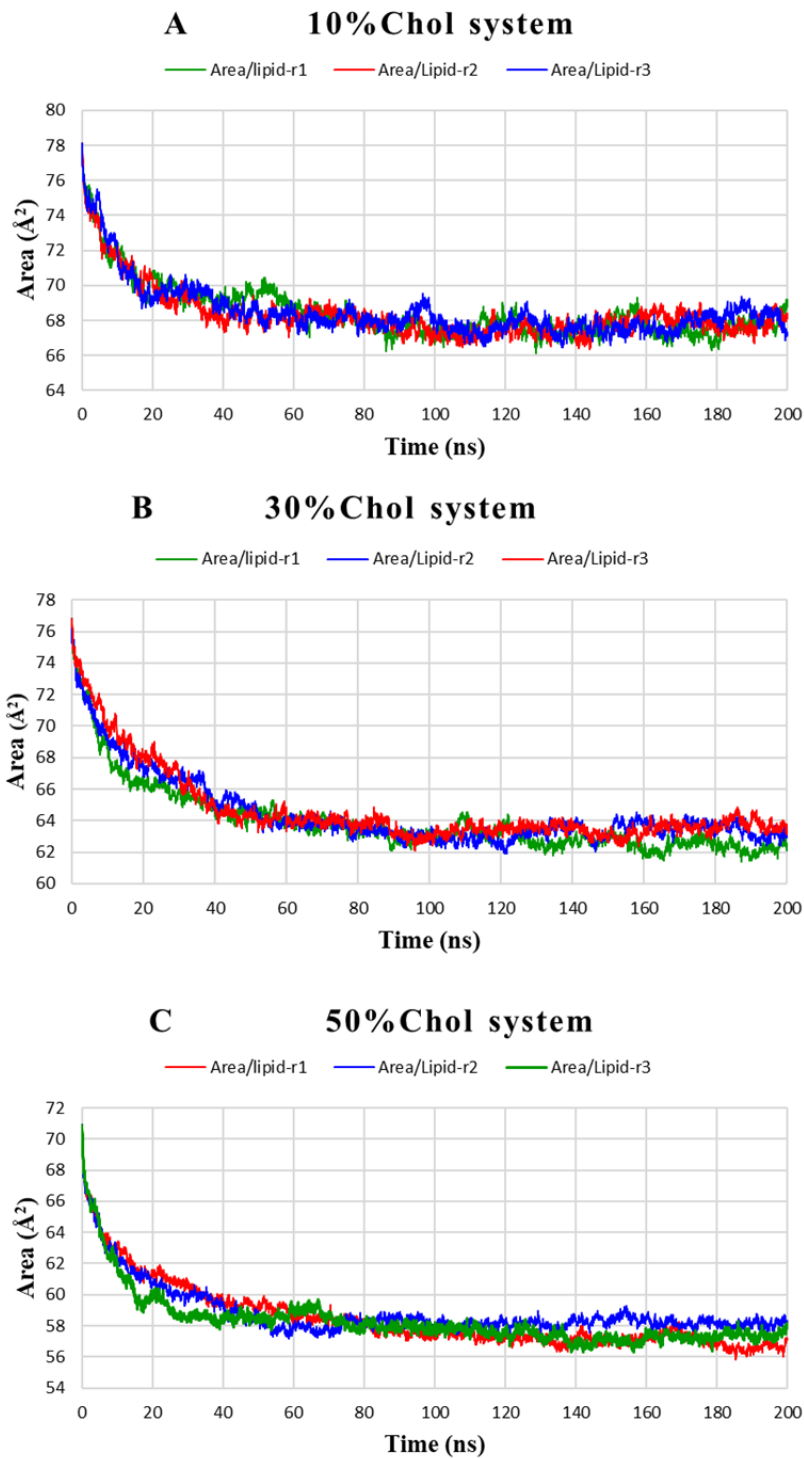


Figure 3.2. *A*, *B* and *C* showing the surface area/lipid values plotted as a function of time for the three replicas of 10%, 30%, and 50% cholesterol systems respectively, in POPC bilayer system.

3.2 Structural changes in the protein during equilibration in the NPT process

3.2.1 Root mean square deviation (RMSD)

To determine the structural variations in the protein over the duration of the simulation, the RMSD of the protein backbone is calculated. It gives a measure of the protein structural changes as shown in Figures 3.5-3.7, for different systems. For the 10% cholesterol system with α HL, within the first 50ns of the simulation, RMSD is reaching a value between 2 and 2.5 Å. From then on, for the next 100ns, protein still fluctuates, and the values reached a fairly stable value between 150 and 200ns. The three replicates for each system have shown good consistency and the standard deviation of the three replicates with a block averaging is of 2.19 ± 0.03 Å. It is also a good indicator that the system has stabilized, and further analysis could be performed.

Similarly, for the 30% and 50% cholesterol systems, RMSD values also vary between 2 and 2.5 Å. Three replicates reach a stable value within the last 50ns of the simulation. For 30% cholesterol system, the average value of RMSD in the last 50ns of the simulation is 2.14 ± 0.02 Å and for 50% cholesterol system, it is 2.14 ± 0.02 Å.

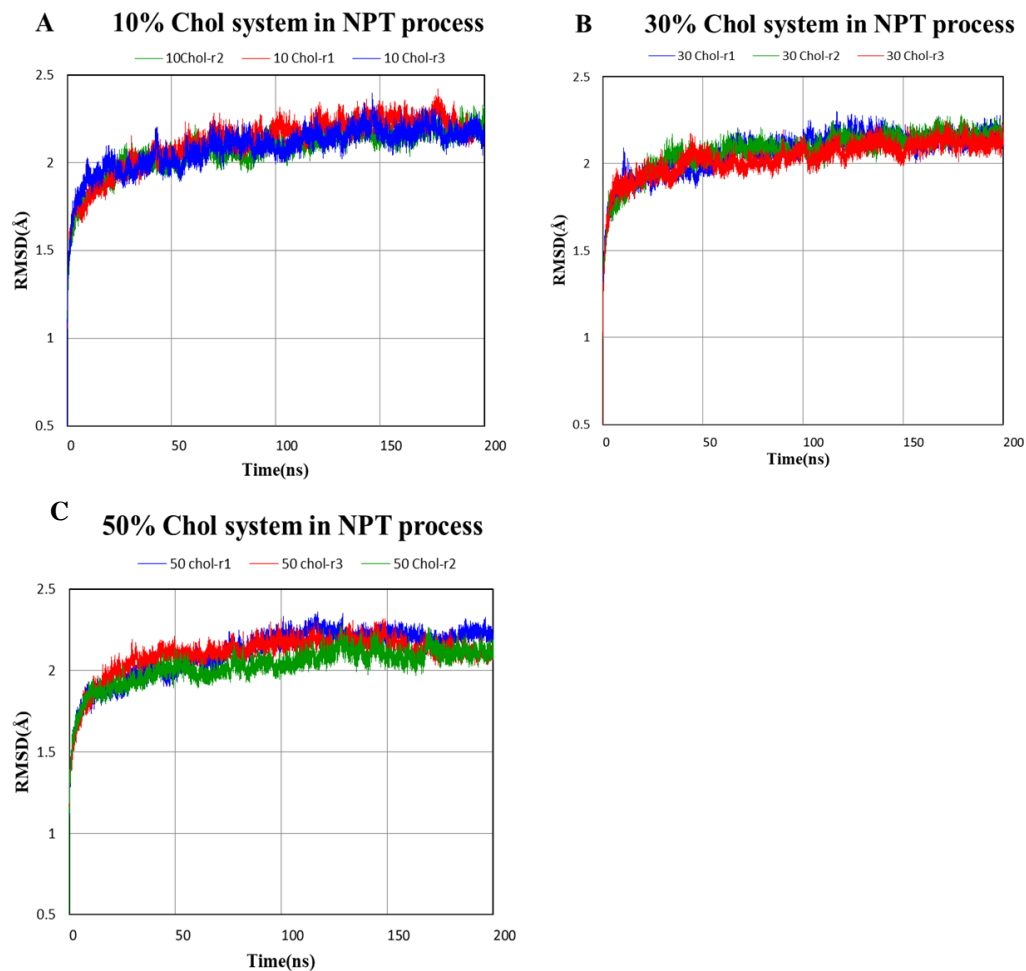


Figure 3.3. *A, B and C* showing the RMSD Vs time for various replicates of the 10%, 30%, and 50% Cholesterol systems respectively, in the NPT process during the 200ns equilibration

3.2.2 Pore radius profiles during equilibration in the NPT process

Pore radius is calculated throughout the progress of the simulation as a function of distance along the Z-axis. This helps in a clear understanding of whether the channel is conducting the ions or there is an occlusion created for the flow of current. Pore radius profiles represented here are for every 20ns of the simulation, but additional curves are included wherever necessary.

Figure 3.6 indicates the pore radius profiles of the 10% Cholesterol system with its three replicates. From the data, it is evident that the radius between $z = -40 \text{ \AA}$ and $z = -25 \text{ \AA}$ where the β -barrel(pore region of the protein) is located, fluctuations are very high and the pore radius has a minimum of 6 \AA during the course of the simulations in most of the systems. These minimum values are not altered much during the simulation. However, the three replicates have different variations in terms of the channel radius. Replicate 1 has shown a considerable variation compared to that of replicates 2 and 3. Apart from the fluctuations in the β -barrel structure, the presence of charged residue loops connecting the β -barrel strands at the trans(bottom) entrance of the protein may cause additional constriction (constriction 2 in Figure 3.4) to the current through the channel.

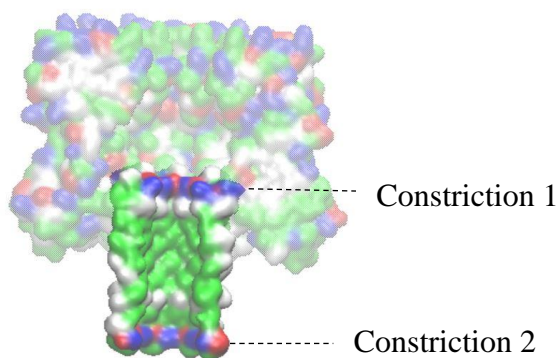


Figure 3.4 showing the structure of pore and charged residues in the pore (represented in red and blue) that might cause additional constriction. Constriction point 1 is the entrance of the pore caused due to charged residues lysine(blue) and glutamic acid(red); constriction 2 is the at the trans-entrance of the pore, formed by charged residues(lysine(blue) and aspartic acid(red)) connecting the β -sheets.

For the 30% cholesterol system, pore radius profiles of all the replicates are represented in Figure 3.7. Run-2 for the 30% cholesterol system has more fluctuations as the

simulation progresses and reached a steady value at around 130ns. Fluctuation in 30% cholesterol systems is greater than those in 10% cholesterol systems, as observed from the pore radius profiles.

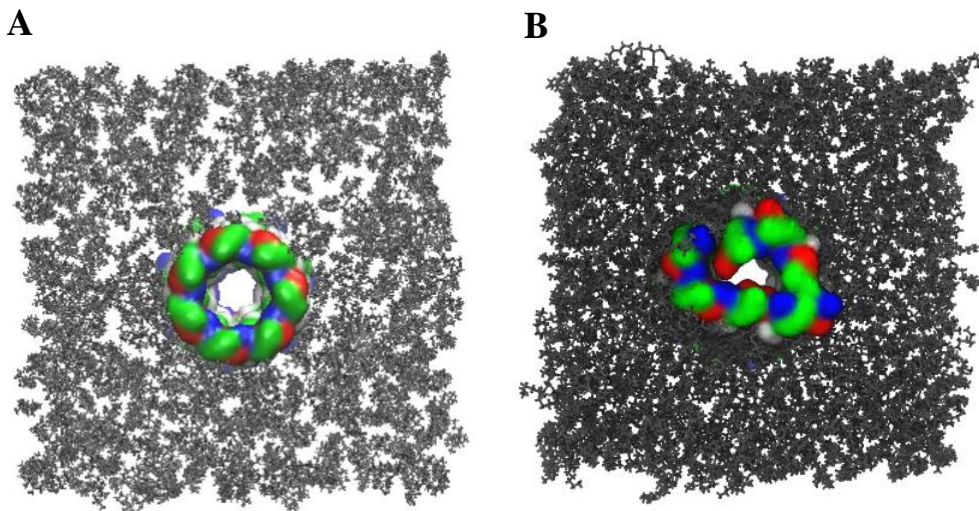


Figure 3.5 indicating the first replica of 50% cholesterol system showing the trans entrance of the pore **A**) before the simulation **B**) and channel occlusion after the electric field is applied. Also, observed is a visible membrane relaxation

Similar to the 10% and 30% systems, pore radius profiles for the 50% cholesterol system in the NPT process. Systems ran for 200ns in NPT process for equilibration. First replicate has shown more fluctuations than the other two. It has shown a fluctuation in the pore radius from around 8.5 Å at 30ns to closure of ≈ 3.7 Å by 180ns of the simulation. The other replicas also have shown a considerable reduction in the pore radius to around 6 Å. This reduction in the pore radius could lead to a reduction in the current through the pore. This might be because the increase in the cholesterol concentration would reduce the fluidity of the membrane which might in turn affect either the ability of the α HL to insert initially or to develop a stable ion

conducting protein channel in the membrane.²³ When the systems stabilized, the electric field is applied in the next step for evaluating the ionic current through the pore of the simulation. Pore radius profiles during the NVT process are in section 3.3.

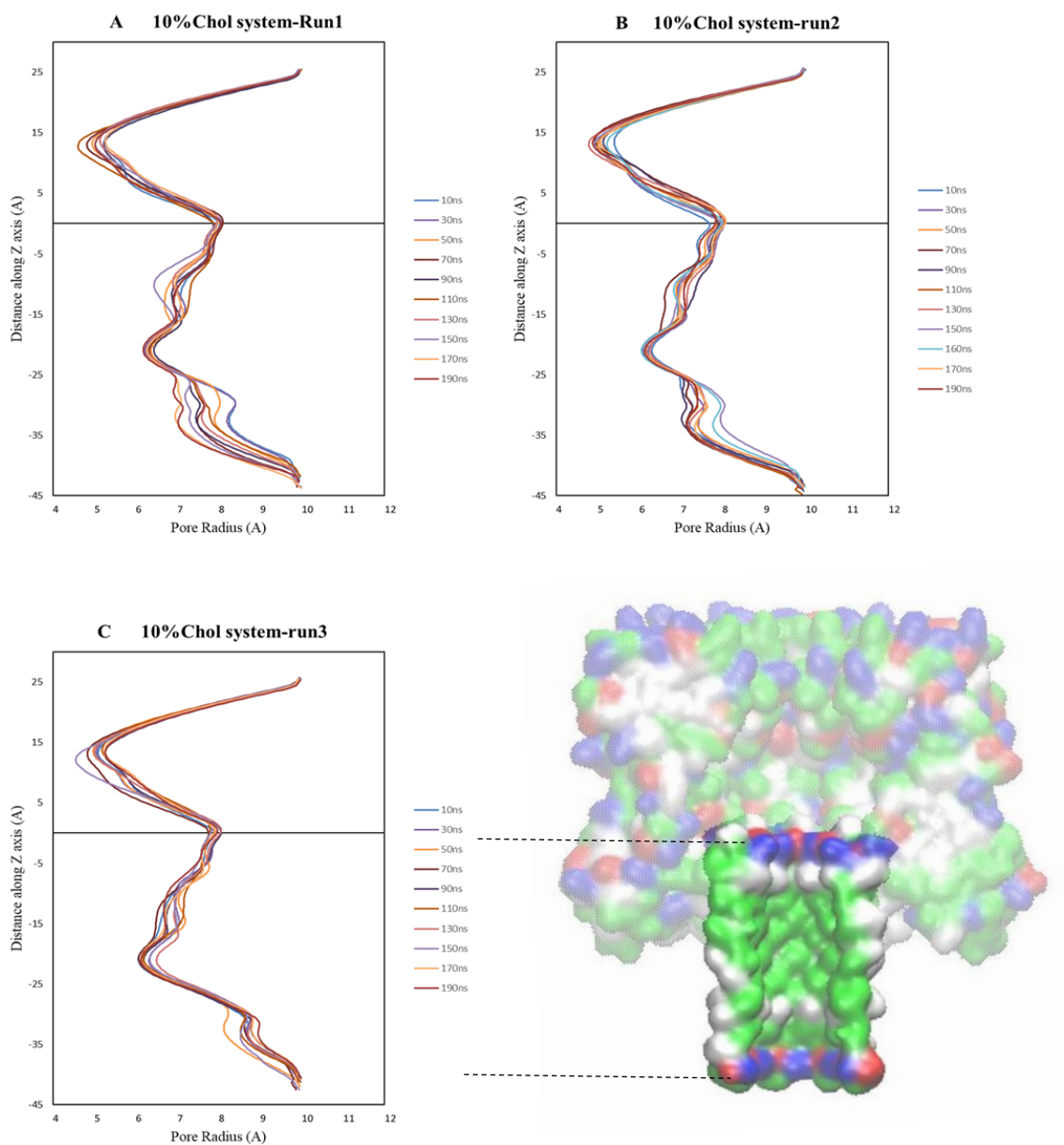


Figure 3.6. *A, B and C* showing the pore radius profiles for the three replicates of the 10% Cholesterol system in the NPT process during the 200ns equilibration. Figure showing the protein pore region (between the dotted lines) within the length of the protein along which pore radius profiles have been plotted

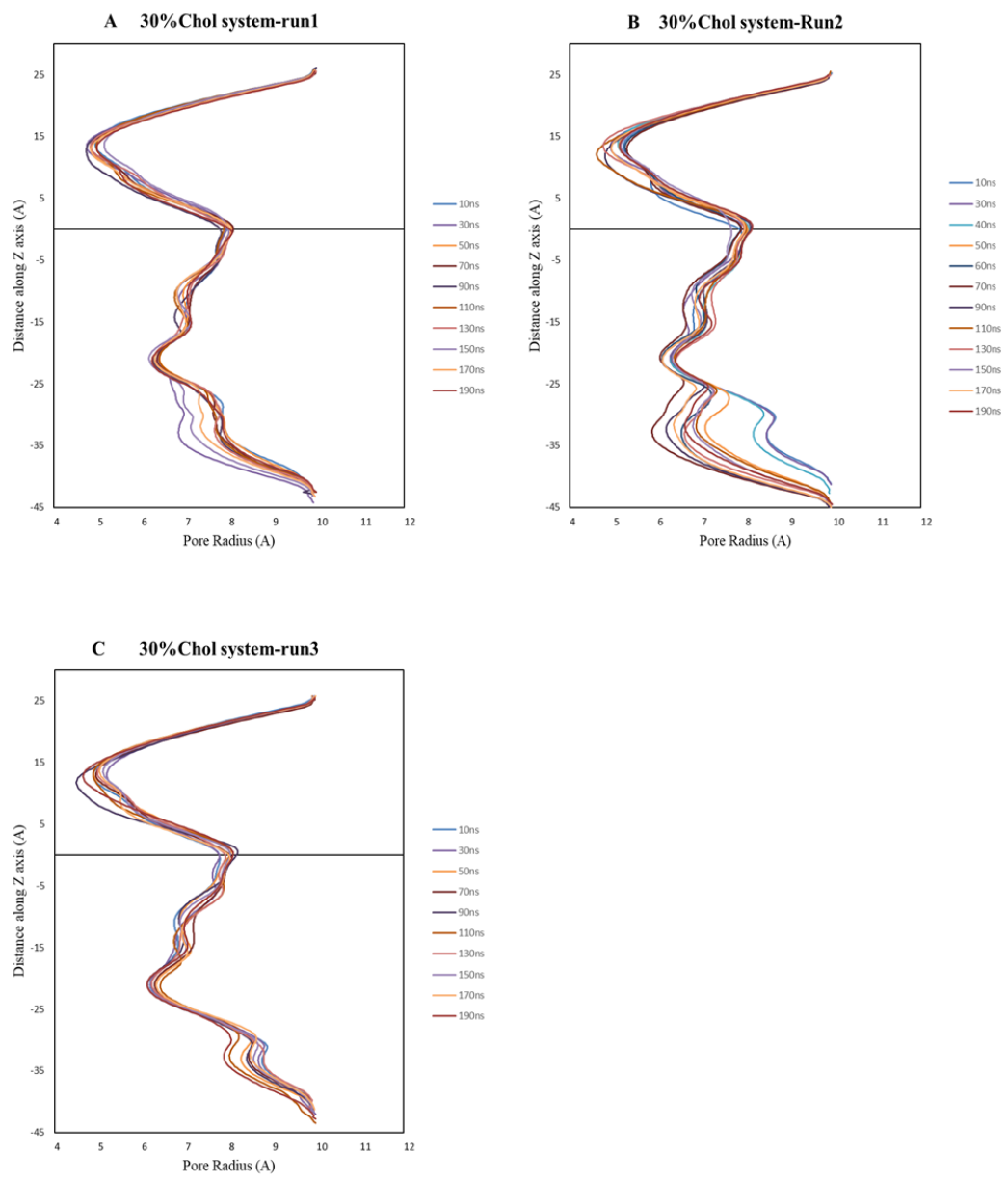


Figure 3.7 showing the pore radius profiles for the three replicates of the 30% Cholesterol system in the NPT process during the 200ns equilibration

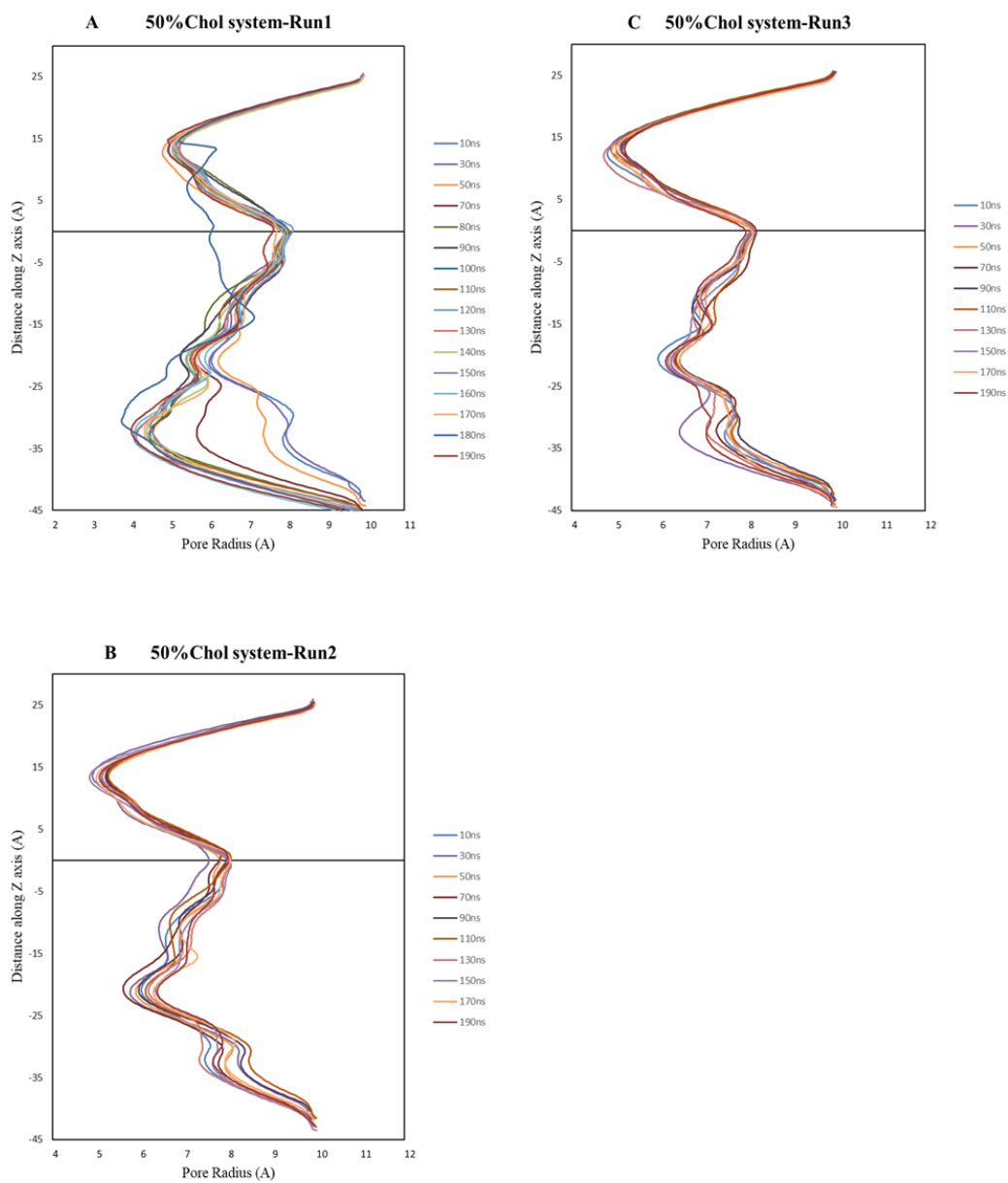


Figure 3.8 showing the pore radius profiles for the three replicates of the 50% Cholesterol system in the NPT process during the 200ns equilibration

3.3 Structural changes in the protein during equilibration in NVT process

Similar to the NPT process, pore radius profiles were evaluated for the systems with an electric field applied under NVT conditions and the data is presented in the

current section. Pore radius profiles for the systems and their replicas are shown in Figures 3.10-3.12.

For the 10% cholesterol system, as the simulation progressed, there is a clear occlusion in the pore because of the reduction in the pore radius from 8 Å to 5 Å in replicates-1 and 2 of the system. Replicate 1 has an obstructed pore for about a 100ns time starting at around 60ns of the simulation and stabilized to a pore radius in the range close to 8 Å after that. Similar to replicate 1, replicate-2 also has a reduced pore radius between 50ns and 150ns and stabilized to around 8 Å towards 200ns. The third replicate also has occlusion and the fluctuation in the pore radius between 9 Å and 6.5 Å. The system started to fluctuate after 50ns of the simulation and continued until 150ns, after which it stabilized. Due to the large fluctuations along the pore of the protein, there may be an additional constriction point introduced to the current at the trans-entrance of the protein. Trans-entrance of the protein is composed of charged residues which may undergo structural changes due to structural changes along the length transmembrane region. The pore radius profiles obtained are similar to those obtained by Guros et al.²² in pure POPC membrane without cholesterol. They obtained an average pore radius profile in the range between 5 and 7.5 Å, comparable to the values obtained in cholesterol systems.

For the 30% Cholesterol system, replicates 2 and 3 are fairly stable through the progress of the simulation. Replicate 2 has a pore radius between 5.5 Å and 7 Å while the third replicate has varied between 7.5 Å and 8.5 Å. In contrast, replicate-1 has shown significant fluctuations in the range between 4.7 Å and 8 Å. The fluctuation in the pore radius of this replicate continued until 200ns (decreasing up to 5 Å) of the

simulation and hence an additional 50ns was performed, during which it stabilized to pore radius close to 7.5 Å. The pore radius values to which 30% systems collapsed are in a comparable range to those in 10% system although there is a significant difference in the fluctuation through the progress of the simulation. These values of the pore radius are in a comparable range to the pure POPC system as well.²² This could imply that the percentage of cholesterol might have a regulatory effect on the protein and hence on the functioning of the protein pore.

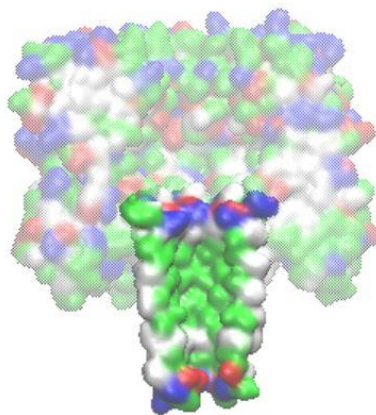


Figure 3.9 showing the pore occlusion in replicate-1 of 50% cholesterol system²⁰ with charged residues(Lysine(blue) and aspartic acid(red)) at the trans-entrance of the pore(constriction point 2) bending inwards, thereby obstructing the ion flow.

Similar to the 10% and 30% cholesterol systems, there is a clear increased fluctuation in the channel radius of 50% cholesterol system. From around 140ns, there is clear channel occlusion for the ion crossing. Further analysis on the current has been provided in the following section in terms of the number of ion crossings across the constriction point of the pore.

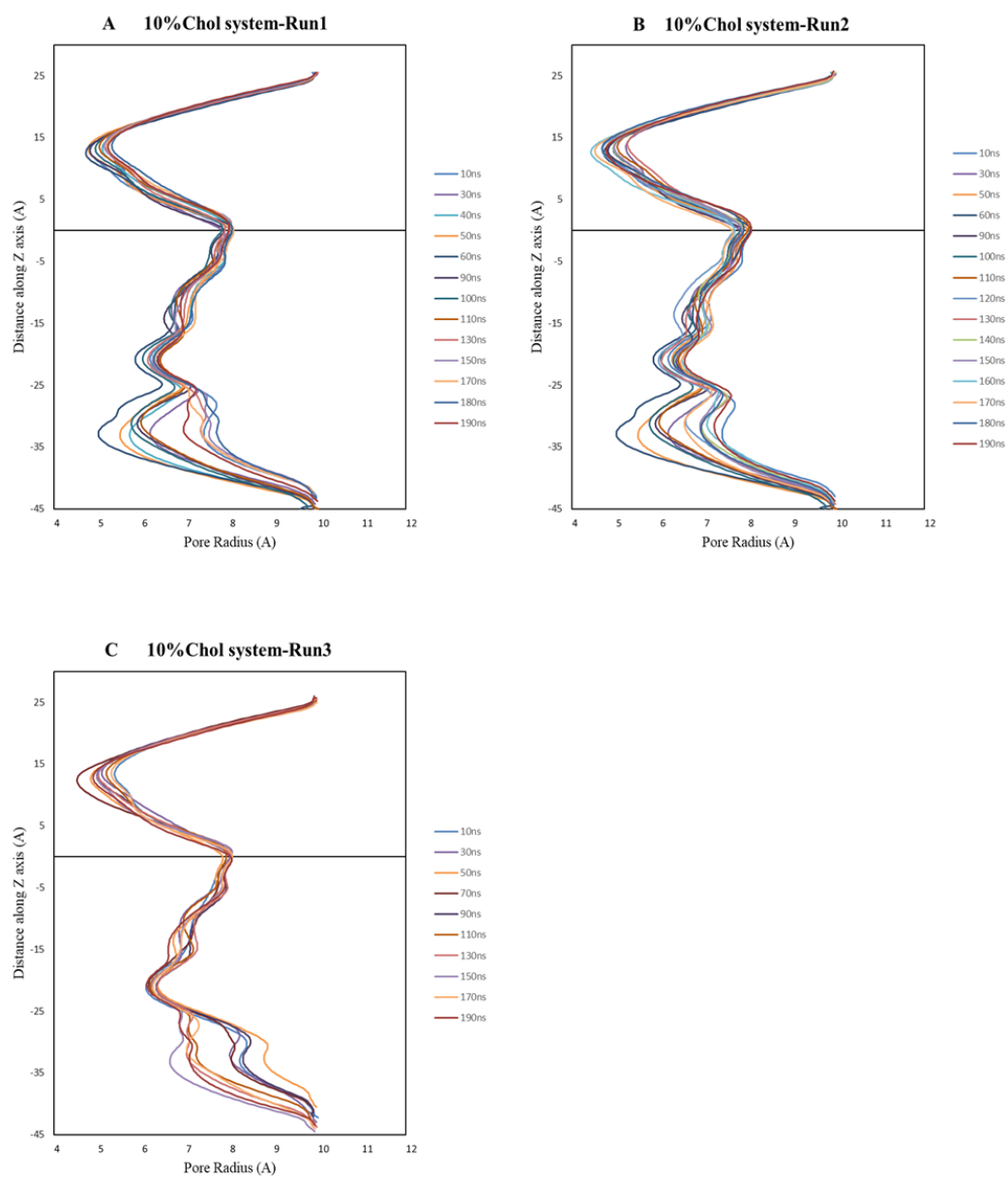


Figure 3.10 showing the pore radius profiles for the three replicates of the 10% Cholesterol system in the NVT process with the electric field on

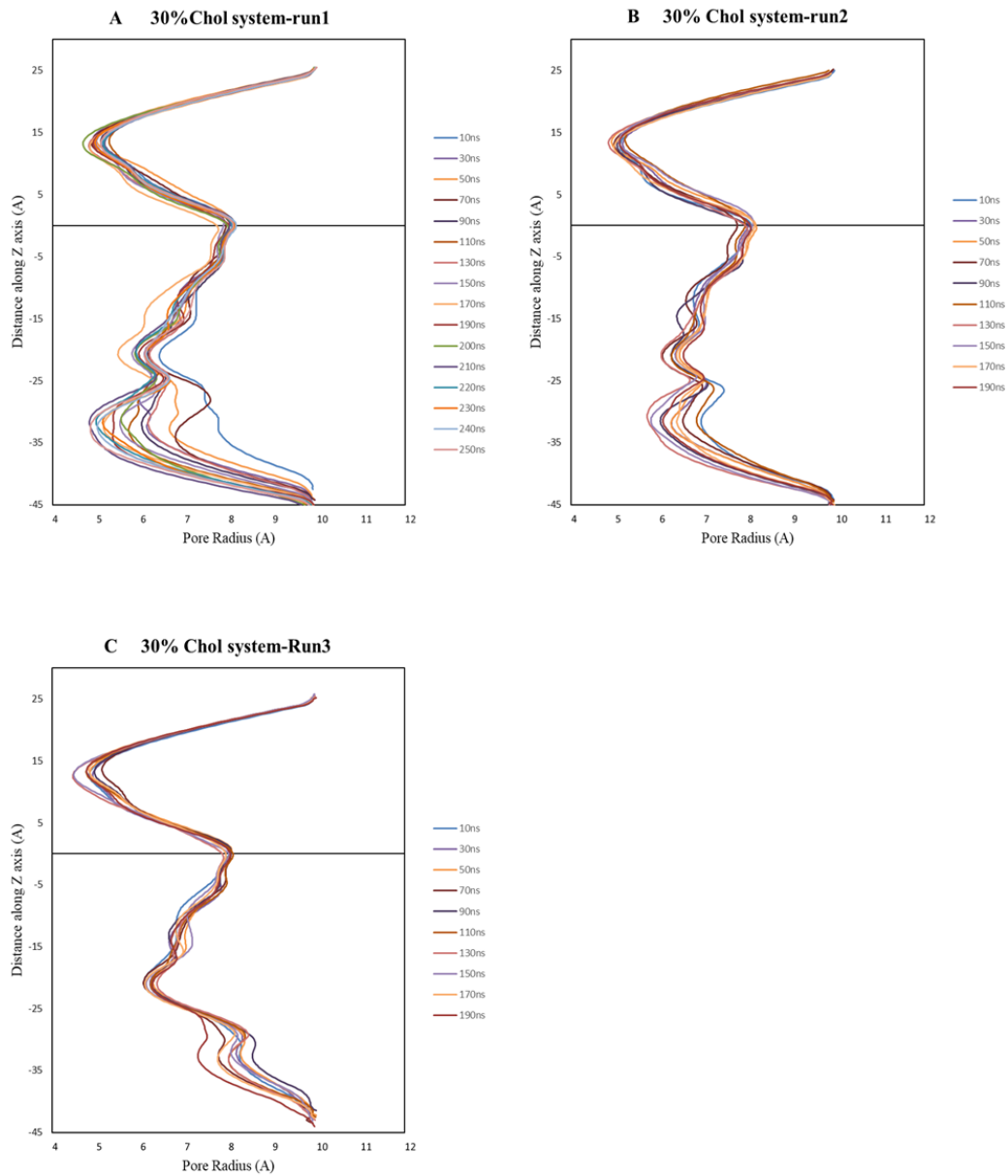


Figure 3.11 showing the pore radius profiles for the three replicates of the 30% Cholesterol system in the NVT process with the electric field on

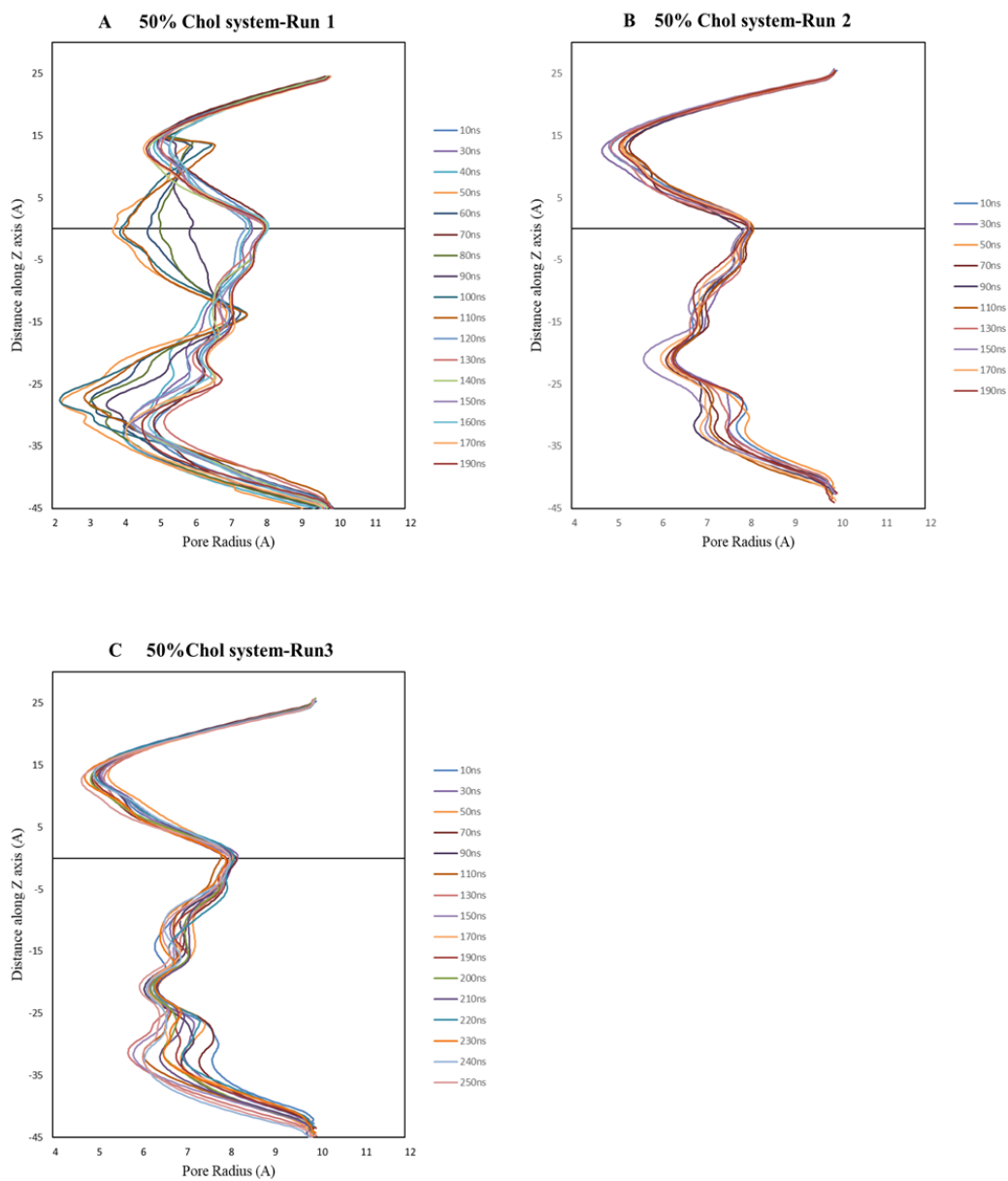


Figure 3.12 showing the pore radius profiles for the three replicates of the 50% Cholesterol system in the NVT process with the electric field on

3.4 Ion conductance

Ion conductance values of the system across the channel of the protein is measured in terms of the number of ion crossing as mentioned in the methods section. Ion current through the channel is primarily calculated through the number of ion

crossing across a reference point, which is placed at the entrance of the pore. Net accumulation of the ions for each system is calculated and presented in Figure 3.10. Current through the pore is presented in Table 3.1.

Table 3.1 Current through the pore of various systems in pA.

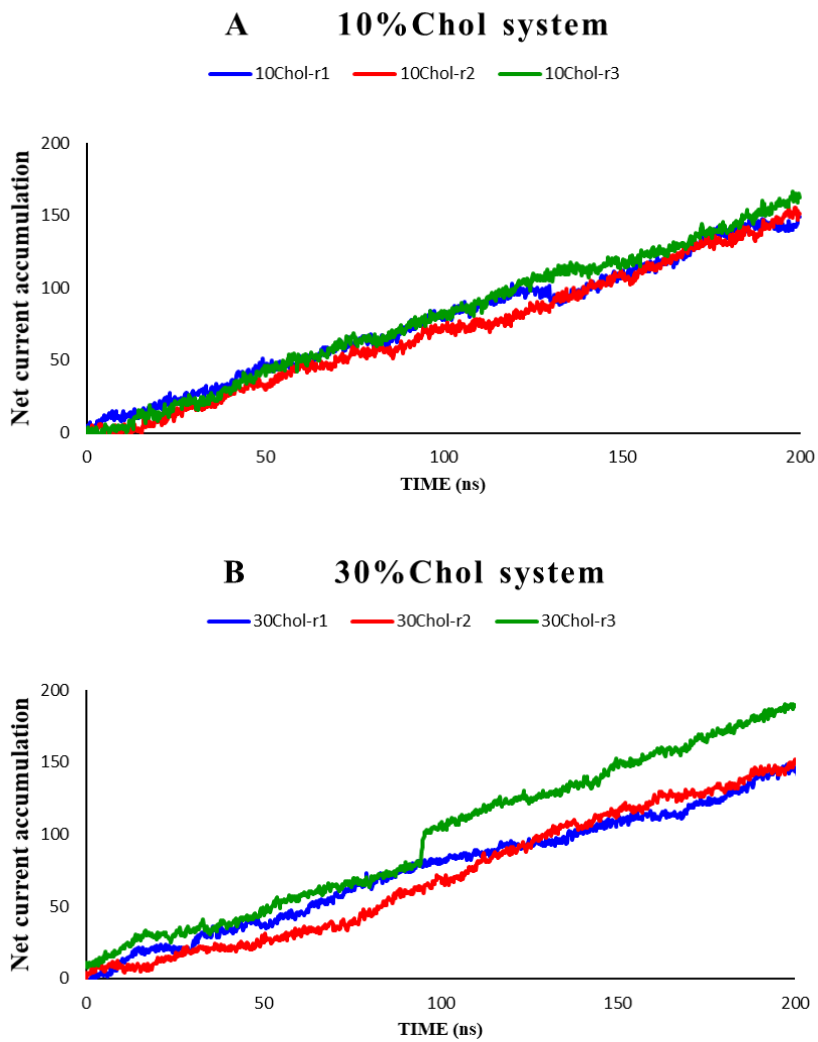
System	Simulation time [ns] with NVT	Channel current through the pore (pA)
10% Chol-run1	200	116.338
10% Chol-run2	200	122.841
10% Chol-run3	200	132.065
30% Chol-run1	250	116.099
30% Chol-run2	200	124.457
30% Chol-run3	200	148.284
50% Chol-run1	200	107.223
50% Chol-run2	200	108.81
50% Chol-run3	250	118.147
Pure POPC-s1 * ²²	200	60.9
Pure POPC-s2 * ²²	200	94.8
Experimental * ⁴⁴	-	150±3

*- indicates the data published previously in pure POPC membrane simulations of α -hemolysin and experimental data published.

Although lipid interactions do not completely occlude the current flow through the pore, their effect is on the current is considerable. 10% cholesterol systems have a current accumulation of around 165 ions by the end of 200ns simulation. The three replicas have shown good consistency.

For 30% cholesterol system, replicate 3 has shown higher current flow than the of the other 2 replicas. Similarly, for 50% cholesterol system, the number of ions that crossed the reference point is less than that of 30% system. The three replicas of 50% cholesterol system have shown good consistency. This is an anomaly observed with respect to the pore radius profiles because there is an additional occlusion in the

channel pore observed in the first replica of the system. The pore occlusion observed is expected to reduce the current through the pore significantly but no such behaviour is observed. Further analysis would be required to understand this unexpected behaviour of the system.



C 50% Chol system

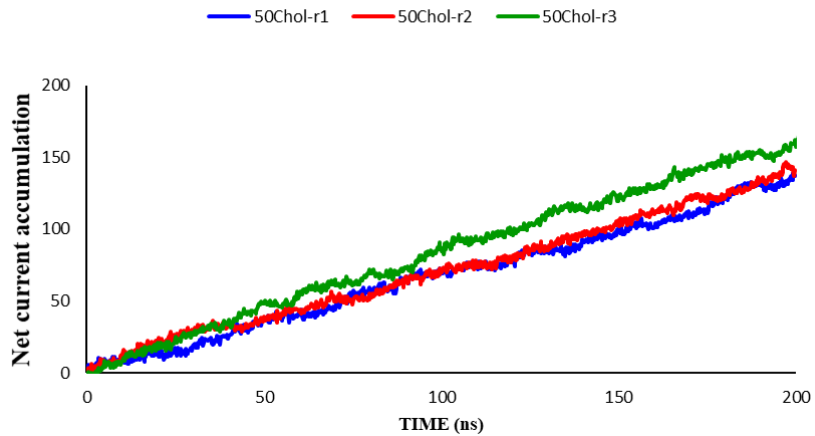


Figure 3.13 showing the net current accumulation for the three replicates of the systems simulated in the NVT process

Chapter 4: Discussion

Membrane equilibration has been measured in terms of surface area/lipid calculations for all the replicates. Guros et al. have established that a 200ns equilibration step is required and sufficient to replicate the experimental conditions using MD simulations of POPC membranes with ion channels.²² All the systems were subjected to 200ns of equilibration step in the NPT process as equilibration for longer times makes the simulations get closer to the experimental conditions. It has been observed in the current thesis, that the three replicas of each system are consistent and converged to the same stable value. The reduction in the surface area with the progress of simulation might be because of the lipids rearranging within themselves and with respect to the protein to adjust to the hydrophobic mismatch. It has also been observed that the surface area/lipid to which the systems converged reduced with increase in the concentration of cholesterol in the membrane.

To monitor the structural changes in the systems, RMSDs were plotted with the first frame of the simulation as the reference. RMSD values of the protein backbone are in the same range of around 2 Å in all the systems. After a 150 ns equilibration step, the values remained stable indicating that the systems can be used for further analysis due to a relaxing of the protein structure.

Pore radius profiles are calculated along the transmembrane region. It has been shown that the lipid bilayer in which the ion channel is placed has an effect on the functioning of the protein channel. This arises because membrane lipids interact with hydrophobic residues on the outside of the transmembrane region and any mismatch in the height causes the hydrophobic residues to rearrange. This causes structural changes

in the protein channel and hence disrupts the current through it. Apart from the constriction caused due to lysine and glutamic acid residues at the entrance of the pore in α HL, hydrophobic mismatch with the inner leaflet of the bilayers causes the charged residues connecting the β -strands at the end of the protein (opposite of the α HL cap near the constriction 2, see Figure 3.4), to undergo structural changes thereby creating another constriction point. Hence, for the effective functioning of the ion channel, the membrane plays an important role.

Also, in the systems, it is observed that there is a considerable reduction in the conductance of protein with 50% cholesterol. The presence of cholesterol decreases the fluidity and permeability of the POPC membrane. There is a clear pore collapse in the replicate 2 shown in Figure 3.5 and 3.6. The reason for the pore collapse might be because, with an increase in the number of cholesterol molecules in the membrane, accessibility to the hydrophobic surface would be reduced. This might have reduced the number of POPC molecules available to interact with hydrophobic residues on the surface of the protein channel or the reduction in lateral diffusion of lipids and hence their interactions with the protein. This reduced accessibility might have caused mismatched hydrophobic effects that lead to the charged residues at the trans-entrance bending inwards causing the pore to collapse and occlude the current. More analysis is needed to further quantify the cause for the pore collapse.

As shown in Table 3.1, current values in terms of pA are presented. Evidently, from the data, there is an increase in the current in cholesterol systems as compared to that of pure POPC systems reported by Guros et al. In the pure POPC systems, current values are measured within the pore while in the current thesis they are calculated at

the entrance of the pore. Initially, it was thought that this might be because of the reference point across which the current values are being monitored. But with different reference points, the current through the pore remained in the same range with very little difference. For the 10% cholesterol system, in accordance with the pore radius profiles, replicate-3 has shown a higher current than the other two. Similarly, in 30% cholesterol system, replicate-1 which has shown the maximum fluctuation has the least current and replicate-3 has the highest current through the pore. For the 50% cholesterol system, currents are comparatively lower than those of the other two systems. Further analysis is required to understand the conductance of the pore despite the observed occlusion in the channel.

Chapter 5: Conclusion and Future work

Effect of cholesterol on the structure and hence function of α HL has been studied. Relaxation in the membrane after 200ns of the simulation was observed and monitored in terms of surface area/lipid. Protein backbone structural changes were monitored during equilibration in the NPT process. It has been concluded that within 150ns, changes in the protein structure are not significant.

In terms of pore radius, apart from the first constriction point at the entrance of the pore, second constriction point at the trans-entrance of the protein was observed. This is due to the inward bending of the residues as a result of hydrophobic mismatch of protein with the inner leaflet of the membrane. The importance of lipid interactions, especially the presence of cholesterol in the membrane has been evaluated. Net current profiles have been evaluated for different systems and the results are presented.

In the future, it would be interesting to further investigate the reason behind the atypical current conductance through the pore and to find the effect of temperature on the behavior of the POPC systems with cholesterol. It would also be interesting to know the effect of curvature in the lipid membrane on the interactions of lipids with the hydrophobic residues on the protein.

REFERENCES

1. van Meer, G.; Voelker, D.; Feigenson, G., Membrane lipids: where they are and how they behave. *Nature Reviews Molecular Cell Biology* **2008**, 9 (2), 112-124.
2. Kukol, A., Lipid Membranes for Membrane Proteins. *Molecular Modeling of Proteins: 2nd Edition* **2015**, 1215, 73-90.
3. Cooper, G. M., Cell Membranes. **2000**.
4. Pike, L., The challenge of lipid rafts. *Journal of Lipid Research* **2009**, 50, S323-S328.
5. Cooper, G. M., Structure of the Plasma Membrane. Sinauer Associates: 2000. (accessed 2000).
6. Dahl, S.; Sylte, I.; Ravna, A., Structures and models of transporter proteins. *Journal of Pharmacology and Experimental Therapeutics* **2004**, 309 (3), 853-860.
7. Li, J.; Wen, P.; Moradi, M.; Tajkhorshid, E., Computational characterization of structural dynamics underlying function in active membrane transporters. *Current Opinion in Structural Biology* **2015**, 31, 96-105.
8. Haque, F.; Li, J.; Wu, H.; Liang, X.; Guo, P., Solid-state and biological nanopore for real-time sensing of single chemical and sequencing of DNA. *Nano Today* **2013**, 8 (1), 56-74.
9. Coulter, W. H. Means For Counting Particles Suspended In A Fluid. US-Patent#2,656,508, Oct. 20, 1953, 1949.
10. Nehra, A.; Ahlawat, S.; Singh, K., A biosensing expedition of nanopore: A review. *Sensors and Actuators B-Chemical* **2019**, 284, 595-622.
11. Arjmandi-Tash, H.; Belyaeva, L.; Schneider, G., Single molecule detection with graphene and other two-dimensional materials: nanopores and beyond. *Chemical Society Reviews* **2016**, 45 (3), 476-493.
12. Lee, K.; Park, K.-B.; Kim, H.-J.; Yu, J.-S.; Chae, H.; Kim, H.-M.; Kim, K.-B., Recent Progress in Solid-State Nanopores. *Advanced Materials* **2018**, 30 (42), 1704680.
13. Krasilnikov, O.; Sabirov, R., Ion-Transport Through Channels Formed in Lipid Bilayers by Staphylococcus-Aureus Alpha-Toxin. *General Physiology and Biophysics* **1989**, 8 (3), 213-222.

14. Schneider, G. F.; Kowalczyk, S. W.; Calado, V. E.; Pandraud, G.; Zandbergen, H. W.; Vandersypen, L. M.; Dekker, C., DNA translocation through graphene nanopores. *Nano Lett* **2010**, *10* (8), 3163-7.
15. van den Hout, M.; Hall, A.; Wu, M.; Zandbergen, H.; Dekker, C.; Dekker, N., Controlling nanopore size, shape and stability. *Nanotechnology* **2010**, *21* (11).
16. Hall, A. R.; Scott, A.; Rotem, D.; Mehta, K. K.; Bayley, H.; Dekker, C., Hybrid pore formation by directed insertion of α -haemolysin into solid-state nanopores. *Nat Nanotechnol* **2010**, *5* (12), 874-7.
17. Wang, J.; Yang, J.; Ying, Y.-L.; Long, Y.-T., Nanopore-Based Confined Spaces for Single-Molecular Analysis. *Chemistry – An Asian Journal* **2019**, *14* (3), 389-397.
18. Gouaux, E., α -Hemolysin from *Staphylococcus aureus*: An Archetype of β -Barrel, Channel-Forming Toxins. *Journal of Structural Biology* **1998**, *121* (2), 110-122.
19. Song, L.; Hobaugh, M. R.; Shustak, C.; Cheley, S.; Bayley, H.; Gouaux, J. E., Structure of Staphylococcal α -Hemolysin, a Heptameric Transmembrane Pore. *Science* **1996**, *274* (5294), 1859.
20. Song, L.; Hobaugh, M.; Shustak, C.; Cheley, S.; Bayley, H.; Gouaux, J., Structure of staphylococcal alpha-hemolysin, a heptameric transmembrane pore. *Science* **1996**, *274* (5294), 1859-1866.
21. Humphrey, W.; Dalke, A.; Schulten, K., VMD: Visual molecular dynamics. *Journal of Molecular Graphics* **1996**, *14* (1), 33-38.
22. Guros, N. B.; Balijepalli, A.; Klauda, J. B., The Role of Lipid Interactions in Simulations of the α -Hemolysin Ion-Channel-Forming Toxin. *Biophys J* **2018**, *115* (9), 1720-1730.
23. Valenzuela, S.; Alkhamici, H.; Brown, L.; Almond, O.; Goodchild, S.; Carne, S.; Curmi, P.; Holt, S.; Cornell, B., Regulation of the Membrane Insertion and Conductance Activity of the Metamorphic Chloride Intracellular Channel Protein CLIC1 by Cholesterol. *Plos One* **2013**, *8* (2).
24. Ulmschneider, J.; Ulmschneider, M.; Di Nola, A., Monte Carlo vs molecular dynamics for all-atom polypeptide folding simulations. *Journal of Physical Chemistry B* **2006**, *110* (33), 16733-16742.
25. Scheraga, H.; Khalili, M.; Liwo, A., Protein-folding dynamics: Overview of molecular simulation techniques. *Annual Review of Physical Chemistry* **2007**, *58*, 57-83.

26. Hollingsworth, S.; Dror, R., Molecular Dynamics Simulation for All. *Neuron* **2018**, *99* (6), 1129-1143.
27. Sagui, C.; Darden, T., Molecular dynamics simulations of biomolecules: Long-range electrostatic effects. *Annual Review of Biophysics and Biomolecular Structure* **1999**, *28*, 155-179.
28. Jo, S.; Kim, T.; Iyer, V. G.; Im, W., CHARMM-GUI: A web-based graphical user interface for CHARMM. *Journal of Computational Chemistry* **2008**, *29* (11), 1859-1865.
29. Jo, S.; Lim, J.; Klauda, J.; Im, W., CHARMM-GUI Membrane Builder for Mixed Bilayers and Its Application to Yeast Membranes. *Biophysical Journal* **2009**, *97* (1), 50-58.
30. Brooks, B.; Brooks, C.; Mackerell, A.; Nilsson, L.; Petrella, R.; Roux, B.; Won, Y.; Archontis, G.; Bartels, C.; Boresch, S.; Caflisch, A.; Caves, L.; Cui, Q.; Dinner, A.; Feig, M.; Fischer, S.; Gao, J.; Hodoscek, M.; Im, W.; Kuczera, K.; Lazaridis, T.; Ma, J.; Ovchinnikov, V.; Paci, E.; Pastor, R.; Post, C.; Pu, J.; Schaefer, M.; Tidor, B.; Venable, R.; Woodcock, H.; Wu, X.; Yang, W.; York, D.; Karplus, M., CHARMM: The Biomolecular Simulation Program. *Journal of Computational Chemistry* **2009**, *30* (10), 1545-1614.
31. Jo, S.; Kim, T.; Im, W., Automated Builder and Database of Protein/Membrane Complexes for Molecular Dynamics Simulations. *Plos One* **2007**, *2* (9).
32. Rose, P. W.; Prlić, A.; Altunkaya, A.; Bi, C.; Bradley, A. R.; Christie, C. H.; Costanzo, L. D.; Duarte, J. M.; Dutta, S.; Feng, Z.; Green, R. K.; Goodsell, D. S.; Hudson, B.; Kalro, T.; Lowe, R.; Peisach, E.; Randle, C.; Rose, A. S.; Shao, C.; Tao, Y. P.; Valasatava, Y.; Voigt, M.; Westbrook, J. D.; Woo, J.; Yang, H.; Young, J. Y.; Zardecki, C.; Berman, H. M.; Burley, S. K., The RCSB protein data bank: integrative view of protein, gene and 3D structural information. *Nucleic Acids Res* **2017**, *45* (D1), D271-D281.
33. Durell, S. R.; Brooks, B. R.; Ben-Naim, A., Solvent-Induced Forces between Two Hydrophilic Groups. *The Journal of Physical Chemistry* **1994**, *98* (8), 2198-2202.
34. Jorgensen, W.; Chandrasekhar, J.; Madura, J.; Impey, R.; Klein, M., Comparison of Simple Potential Functions for simulating Liquid Water. *Journal of Chemical Physics* **1983**, *79* (2), 926-935.
35. Klauda, J.; Venable, R.; Freites, J.; O'Connor, J.; Tobias, D.; Mondragon-Ramirez, C.; Vorobyov, I.; MacKerell, A.; Pastor, R., Update of the CHARMM All-

Atom Additive Force Field for Lipids: Validation on Six Lipid Types. *Journal of Physical Chemistry B* **2010**, *114* (23), 7830-7843.

36. Klauda, J.; Monje, V.; Kim, T.; Im, W., Improving the CHARMM Force Field for Polyunsaturated Fatty Acid Chains. *Journal of Physical Chemistry B* **2012**, *116* (31), 9424-9431.

37. Phillips, J.; Braun, R.; Wang, W.; Gumbart, J.; Tajkhorshid, E.; Villa, E.; Chipot, C.; Skeel, R.; Kale, L.; Schulten, K., Scalable molecular dynamics with NAMD. *Journal of Computational Chemistry* **2005**, *26* (16), 1781-1802.

38. Martyna, G.; Tobias, D.; Klein, M., Constant-Pressure Molecular-Dynamics Algorithms. *Journal of Chemical Physics* **1994**, *101* (5), 4177-4189.

39. Feller, S.; Zhang, Y.; Pastor, R.; Brooks, B., Constant-Pressure Molecular-Dynamics Simulation - The Langevin Piston Method. *Journal of Chemical Physics* **1995**, *103* (11), 4613-4621.

40. Steinbach, P. J.; Brooks, B. R., New spherical-cutoff methods for long-range forces in macromolecular simulation. *Journal of Computational Chemistry* **1994**, *15* (7), 667-683.

41. Ryckaert, J.; Ciccotti, G.; Berendsen, H., Numerical-Integration of Cartesian Equations of Motion of a System with Constraints - Molecular-Dynamics of N-Alkanes. *Journal of Computational Physics* **1977**, *23* (3), 327-341.

42. Darden, T.; York, D.; Pedersen, L., Particle mesh Ewald: An N·log(N) method for Ewald sums in large systems. *The Journal of Chemical Physics* **1998**.

43. Smart, O.; Goodfellow, J.; Wallace, B., The Pore Dimensions of Gramicidin-A. *Biophysical Journal* **1993**, *65* (6), 2455-2460.

44. Balijepalli, A.; Robertson, J. W. F.; Reiner, J. E.; Kasianowicz, J. J.; Pastor, R. W., Theory of Polymer–Nanopore Interactions Refined Using Molecular Dynamics Simulations. *Journal of the American Chemical Society* **2013**, *135* (18), 7064-7072.